ARTICLES

Spherical Electron Cloud Hopping Molecular Dynamics Simulation on Dissociative Recombination of Protonated Water

Hua-Gen Yu*

Department of Chemistry, Brookhaven National Laboratory, Upton, New York 11973-5000

Received: March 6, 2009; Revised Manuscript Received: May 1, 2009

Dissociative recombination (DR) of H_3O^+ with electrons at zero collision energy has been studied by a direct ab initio molecular dynamics method on four low-lying electronic states of the system. Initial conditions for trajectories are determined by a spherical electron cloud hopping (SECH) model, while nonadiabatic effects are considered through a surface hopping scheme. The energies, forces, and nonadiabatic coupling strengths (NACS) used in trajectory propagations are calculated on-the-fly via state-average complete active self-consistent field (CASSCF) theory with full valence electrons. Dynamics results show that the H_3O^+ DR is ultrafast and yields diversity of products. Product branching fractions are predicted to be 0.660 for (OH + 2H), 0.230 for (H_2O + H), 0.108 for (OH + H_2), and 0.002 for (O + H + H_2), which are in excellent agreement with the heavy-ion storage ring experimental results. Kinetic energies of the eliminated hydrogen atoms are large and show a bimodal distribution.

Introduction

Dissociative recombination (DR)[1−6] is a very important process in interstellar clouds, the upper atmosphere of Earth, plasmas, and high-temperature combustion environments. In interstellar mediums, DR is the main ion neutralization pathway, creating many diverse neutral molecules. DR processes also determine the abundances of molecules. Since the early 1990s, experimentalists can more precisely measure both rate coefficients and product branching ratios of DR due to the advent of advanced techniques including crossed and merged beam methods, flowing afterglow techniques, and heavy-ion storage rings. Results commonly show that DR is nonstatistical for product branching ratios. Such a finding provides a solid explanation for the mystery of the anomalous abundance of those less stable molecules in interstellar clouds.[5]

Although several powerful quantum dynamics algorithms have been developed by use of *R*-matrix theory,[7] multichannel quantum defect theory (MQDT),[4,8,9] and time-dependent wave packet (TDWP) methods[10−16] to calculate the DR cross sections, in contrast, theoretical studies on the product branching ratios of DR are rather limited. Only a couple of triatomic molecular ions such as H_3^+ and HCO^+ ions[12,17−19] have been investigated by quantum dynamics methods with the prediction of product branching ratios. Nevertheless, the theoretical product branching ratios for DR of H_3^+ are still controversial; for example, see the most recent summary addressed by Larsson et al.[20] Therefore, it is very challenging to theoretically study the DR product branching ratios of polyatomic systems by quantum dynamics methods. The difficulty arises from the high-dimension problem, the nonadiabaticity, and the large energy span in DR. In addition, a few direct ab initio molecular dynamics simulations have been carried out for H_3O^+, [21−24] $HCNH^+$,[25,26] and CH_5^+[27] by use of classical mechanics. Calculations of Tachikawa et al.[21,25,27] were performed on the ground electronic states of molecules, whereas those of Taketsugu and co-workers[22,23,26] were done on a set of adiabatic states, including nonadiabatic effects. However, the initial conditions[21,25,26] for trajectories were prepared according to a vertical attachment approximation of electron to the molecular ions, in which the electron excess energies in DR were released via a radiation process. Therefore, those simulations are not really equivalent to the DR processes but the radiative DR, because the total energy of the system is less by an amount of the excess energy than the initial scattering one in molecular dynamics simulations. In other words, the outcomes might not be comparable to experiments. For instance, the molecular dynamics study[21] of the H_3O^+ DR predicted that the H_2O + H products were most likely, in contradiction to experiments[28−31] which showed that the OH + 2H products dominate. For the DR of H_3O^+, a crucial improvement has been made by Kayanuma et al.,[22] who started trajectories on a Rydberg state that is accidentally degenerate with the energy level of e^- + H_3O^+. As a result, the outcomes are in much better agreement with the experiments.

In order to consider the electron excess energy in DR, recently, I have developed a spherical electron cloud hopping (SECH) model[32] for the initial conditions of molecular dynamics trajectories, where a surface hopping algorithm was used to take the nonadiabaticity into account. The preliminary application for the DR of CH^+ and H^+ $(H_2O)_3$ is promising. In particular, the results demonstrated that it is crucial to include the excess energy of scattered electron in dynamics simulations. In this work, we will apply this SECH molecular dynamics method to revisit the dissociative recombination of H_3O^+ at zero collision energy. The current research will focus on the product branching fractions, dissociation dynamics mechanisms, and kinetic energy

* E-mail hgy@bnl.gov; fax +1-631-344 5815.

10.1021/jp902063w CCC: $40.75
Published on Web 05/26/2009

distribution of escaped hydrogen atoms. A comparison with previous theoretical calculations and experiments will be made.

2. Computational Methods

DR of H_3O^+ was studied by the SECH molecular dynamics (MD) method,[32] which has been implemented in the DualOrthGT program.[32−35] As the method has been well described in the literature, no more detail will be given here. Briefly, the SECH MD method considers the DR of H_3O^+ as two consecutive steps. The first step involves a deep electron capture of the ion, which was treated by the SECH model. The next step is the dissociation of the neutral H_3O radical on its electronic valence states. In calculations, four low-lying doublet electronic states were included. It is worthwhile to mention that the SECH MD method addresses only on the product branching ratios at zero collision energy rather than the scattering cross sections. And Rydberg states of H_3O are considered as loose reactants: $e^- + H_3O^+$. The H_3O molecule in a Rydberg state might undergo an autoionization process to become $e^- + H_3O^+$. However, this process would not contribute to the product branching ratios of H_3O^+ DR but influence the capture cross sections. Since H_3O in a Rydberg state never directly dissociates into neutral atom or molecular moieties, it is not necessary to include Rydberg states in the SECH MD calculations. On the other hand, the effect of Rydberg states on dynamics is implemented with the initial conditions of trajectories.

The dissociation dynamics were carried out by the quasiclassical trajectory (QCT) approach, only on a single potential energy surface. But the nonadiabaticities are described by the "fewest switches" surface hopping algorithm.[36] The probability of surface hopping from the kth electronic state to the jth state within the time step Δt is evaluated by

$$P_{kj}(t) = \frac{2\Delta t}{|c_k|^2}\left\{\frac{1}{\hbar} Im(c_k c_j^* V_{jk}) - Re(c_k c_j^* \tau_{jk})\right\} \quad (1)$$

where $V_{ij} = \langle \psi_i(\mathbf{r};\mathbf{R})|\hat{H}_e(\mathbf{r};\mathbf{R})|\psi_j(\mathbf{r};\mathbf{R})\rangle$ are the potential energy matrix elements with $\mathbf{r}$ and $\mathbf{R}$ being the electronic and nuclear coordinates, respectively. Without any higher-order coupling as in this case, the potential matrix $\mathbf{V}$ is diagonal in the adiabatic representation. The nonadiabatic coupling strengths are given by

$$\tau_{kj} = \dot{\mathbf{R}} \cdot \mathbf{d}_{kj} \quad (2)$$

with the atomic velocities $\dot{\mathbf{R}}$ and the nonadiabatic transition matrix elements

$$d_{ij}(\mathbf{R}) = \langle \psi_i(\mathbf{r};\mathbf{R})|\nabla_R \psi_j(\mathbf{r};\mathbf{R})\rangle \quad (3)$$

$c_i(t)$ are the complex electronic amplitudes of the total electronic wave function $\Psi(t)$ $(= \sum_i c_i(t)\psi_i)$ in the adiabatic electronic states $\{\psi_k;\ k = 1-4\}$. Surface hopping is invoked when $P_{kj}(t)$ is greater than a uniform random number generated between 0 and 1. As usual, if surface hopping occurs at time t, the atomic kinetic energies are then adjusted by scaling the mass-weighted atomic velocities in the direction of the nonadiabatic coupling vector at the hopping position of H_3O to conserve the total energy of the system.

Trajectories are propagated by use of a fourth-order symplectic integrator[37] with a time step $\Delta t = 0.043$ fs. At the meantime, the total electronic wave function is computed in the adiabatic representation by solving the time-dependent Schrödinger equation:

$$\dot{c}_k = -\sum_{j=1}^{N} (iV_{kj}/\hbar + \tau_{kj})c_j \quad (4)$$

Energies, forces, and transition matrix elements used in trajectories were computed on-the-fly by the state-average complete active self-consistent field (CASSCF) theory,[38] together with a 6-311G(d,p) basis set.[39] The CASSCF method contains seven electrons and six orbitals, that is, a CAS(7,6)/6-311G(d,p) method. The full valence electrons are active in self-consistent field calculations so that all possible dissociation limits of H_3O can be described correctly. In order to save computational times, following the previous work of Taketsugu and co-workers[22,23,26] the surface hopping is limited among the propagating state and its two adjacent states in energy. A propagating state is the electronic state on which the trajectory is running at time t. Therefore, the propagating state varies with time. Under such a constraint, only the nonadiabatic coupling matrix elements between the propagating state and its two neighboring states are required instead of the whole coupling matrix. This should be a good approximation because those excluded states have a larger energy gap from the propagating state. Due to the large energy gaps, their nonadiabaticities with the propagating state are normally small according to the Massey parameter.[40]

Initial conditions for each trajectory were determined by the SECH model. First, the atomic positions ($\mathbf{R}$) and temporary momenta (p_i) of H_3O^+ were selected according to the canonical ensemble at temperature $T = 298$ K, where the orientation, rovibrational energy, and phases of the ion were randomly sampled. At the positions $\mathbf{R}$, we then calculated the vertical affinity potentials ($E^V_{AP,k}$) of H_3O^+ to the kth ($k = 1-4$) state of H_3O by

$$E^V_{AP,k} = V^{H_3O^+}(\mathbf{R}) - V_k^{H_3O}(\mathbf{R}) \quad (5)$$

where $V^{H_3O^+}$ and $V_k^{H_3O}$ are the adiabatic potential energies of H_3O^+ and H_3O in the kth electronic state, respectively. According to the SECH probability $P_k = \tilde{P}_k/\sum_{i=1}^{N} \tilde{P}_i$, of the incident electron hopping from the ion to the kth electronic state of H_3O, one samples an electronic state j of H_3O through a uniform random number $\zeta \in (0,1)$ and then sets the initial electronic amplitudes as $c_i(t = 0) = \delta_{ij}$ $(i = 1, ..., N)$. The jth state is selected if the condition

$$\sum_{i=1}^{j-1} P_i < \zeta \le \sum_{i=1}^{j} P_i \quad (6)$$

is satisfied. The unnormalized probability is defined as

$$\tilde{P}_j(E^V_{AP,j}) = \begin{cases} g_e/[E^V_{AP,j} - E^0_R + \varepsilon] & \text{if } E^V_{AP,j} \ge 0 \\ \dfrac{g_e \exp[E^V_{AP}/(E^k_{vib} + \varepsilon)]}{[\varepsilon - (E^V_{AP,j} - E^0_R)]} & \text{if } -E^k_{vib} \le E^V_{AP,j} < 0 \\ 0 & \text{otherwise} \end{cases} \quad (7)$$

with

$$E_{\mathrm{R}}^{0} = \min\{0, V^{\mathrm{H_3O^+}}(\mathbf{R}) - V_{\mathrm{Ry}}^{\mathrm{H_3O}}(\mathbf{R})\} \tag{8}$$

where $g_e = 2$ is the electronic statistical factor and $V_{\mathrm{Ry}}^{\mathrm{H_3O}}$ is the potential energy of H_3O in the lowest Rydberg state that is not included in the trajectory calculations. E_{vib}^{k} is the vibrational kinetic energy of H_3O^+. This vibrational energy is an upper limit that could help an incident electron hopping to a higher energy state of the neutral molecule from the ionic state. The infinitesimal $\varepsilon = 10^{-8}$ is used to avoid numerical overflow. In this work, the SECH probability is proportional to the density (ρ) of states at an electron excess energy $E_{\mathrm{AP}}^{\mathrm{V}}$ with an equal width approximation. On the basis of the electron charge (q) interaction potential, the classical density of states is $\rho(E) = q/E$, where the dynamics of the $e^- + H_3O^+$ (for a given geometry) is considered in a full classical mechanics with a continuum energy. The final result in eq 7 is obtained by using an energy shift owing to the exclusion of Rydberg states in trajectory calculations and by multiplying an exponential factor for the electron tunneling effect in the case with $E_{\mathrm{AP}}^{\mathrm{V}} < 0$. Of course, a better SECH probability can be determined by doing quantum scattering calculations.[41,42]

In the SECH model, the excess potential energy $E_{\mathrm{AP}}^{\mathrm{V}}$ of the incident electron has been converted into the atomic kinetic energy in H_3O as

$$\begin{aligned} E_{\mathrm{kin}}^{\mathrm{H_3O}} &= E_{\mathrm{kin}}^{\mathrm{H_3O^+}} + E_{\mathrm{AP}}^{\mathrm{V}} \\ &= \sum_i \frac{(p_i + t_s f_i)^2}{2m_i} \end{aligned} \tag{9}$$

to conserve the total energy, where p_i are the old momenta of atoms with masses m_i. t_s is a scaling parameter of dimension time. The atomic driving force components f_i are defined as[32]

$$f_i = f_i^{\mathrm{e-H_3O^+}}(R_{\mathrm{eM}}^{\mathrm{c}};\mathbf{R}) - f_i^{\mathrm{H_3O}}(\mathbf{R}) \tag{10}$$

The term $f_i^{\mathrm{H_3O}}(\mathbf{R})$ refers to the atomic forces of H_3O at the positions $\mathbf{R}$, while $f_i^{\mathrm{e-H_3O^+}}(R_{\mathrm{eM}}^{\mathrm{c}};\mathbf{R})$ denotes the atomic forces of the $e^- - H_3O^+$ system at both $\mathbf{R}$ and $R_{\mathrm{eM}}^{\mathrm{c}}$. $R_{\mathrm{eM}}^{\mathrm{c}}$ is a critical distance at which the potential energy of H_3O in the selected state will match the potential energy of the $e^- - H_3O^+$ interaction system (In the case with a negative $E_{\mathrm{AP}}^{\mathrm{V}}$, one may flip the standard fractional point charges to be positive to take the repulsive feature in the $e^- - M^{+q}$ system into account.) Both forces were computed by the CASSCF method with/without the fractional point charges. For more detail, the reader can refer to ref 32.

As indicated by Kayanuma et al.,[22] the CASSCF method poorly balances the correlation energy between H_3O^+ and H_3O because of the different number of electrons. As a result, their relative energy cannot be accurately represented by a consistent CASSCF approach. In order to get better vertical potential energies, instead of the CAS(6,6)/6-311G(d,p)[39] method, we used the CAS(2,2)/6-31G(d) method to compute the potential energy surfaces and forces of both H_3O^+ and $e^- - H_3O^+$ systems. The specific combination was selected by comparing the equilibrium geometry of H_3O^+ and its vertical affinity potentials with those calculated with a high-level ab initio method CCSD(T)/aug-cc-pVTZ, that is, the coupled-cluster method with single and double excitation terms and a perturbative triple excitation correction [CCSD(T)][43] together with the aug-cc-pVTZ basis set of Dunning.[44] Such a modification will substantially improve the energetics of the DR of H_3O^+. In particular, one should notice that the CAS(2,2) method is used only for the initial conditions of H_3O^+ while the trajectory calculations are performed by use of the full valence electron CAS(6,7) method. At the beginning of each trajectory, the H_3O^+ ion vibrates near its equilibrium structure, where the potential energy surface of CAS(2,2) is as good as that of CCSD(T) except for a vertical energy shift. Therefore, it is a good approach to use the CAS(2,2) method for the initial conditions.

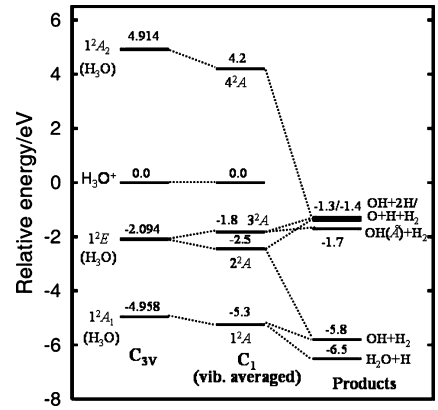

Figure 1. Schematic energy diagram for DR of H_3O^+, where the energies are relative to the ground state of the cation. The four electronic states of H_3O involved in dynamics calculations are shown. Please note that the correlation lines linking to the product channels are not complete.

Trajectories were terminated once two fragments has separated apart by $18.0a_0$. The fragments were analyzed by the graph theory.[34] The critical nuclear distances used are $R_{\mathrm{OH}} = 4.5a_0$ and $R_{\mathrm{HH}} = 3.5a_0$. All electronic structure calculations were performed with the Molpro program package.[45]

3. Results and Discussion

The CAS(2,2)/6-31G(d) method gives an electronic energy of −76.306 734 89 au for the ground-state H_3O^+ (X^1A_1) with the equilibrium geometries $R_{\mathrm{OH}} = 0.9705$ Å and $\theta_{\mathrm{HOH}} = 111.7°$ in C_{3v} symmetry. At the CAS(7,6)/6-311G(d,p) level of theory for H_3O, as shown in Figure 1, the vertical affinity potentials ($E_{\mathrm{AP}}^{\mathrm{V}}$) of H_3O^+ to the low-lying doublets of H_3O are 4.958, 2.094, 2.094, and −4.914 eV in order of energy. The second and third electronic states are the doubly degenerate E state. It will split into two A states in C_1 symmetry, where most trajectories are vibrationally sampled. As a result, there are four vibrationally averaged levels. Three of them are shown in Figure 1. In order to check the accuracy of the hybrid CAS approach, we have optimized the equilibrium structure of H_3O^+ with the high-level ab initio method CCSD/aug-cc-pVTZ. It gives the equilibrium geometries as $R_{\mathrm{OH}} = 0.9758$ Å and $\theta_{\mathrm{HOH}} = 111.7°$ with a vertical affinity potential of 5.208 eV for the ground state of H_3O. At the CCSD geometry, we have also refined the electronic energy with the CCSD(T)/aug-cc-pVTZ method. The CCSD(T) method predicts a vertical affinity potential (H_3O^+) of 5.261 eV correspondingly. It clearly shows that the CAS results are in good agreement with the CCSD/CCSD(T) ones for the equilibrium geometry of H_3O^+ and its vertical affinity potential to the ground-state H_3O. Therefore, such a combination of CAS methods is an acceptable approach for studying the DR of H_3O^+.

For DR of H_3O^+, there are four open product channels at zero collision energy:[22,23]

$$\begin{aligned} H_3O^+ + e^- &\rightarrow H_2O + H \\ &\rightarrow OH + H_2 \\ &\rightarrow OH + 2H \\ &\rightarrow O + H + H_2 \end{aligned} \quad (11)$$

where the (H_2O + H) and (OH + H_2) channels are favorable in energy whereas the other two channels are less preferable. In this work, a total of 500 good trajectories were run. Their total energies are conserved within an error of 0.05 eV, or about a 0.4% error bar of total energy. Those bad trajectories, mostly owing to the convergence problem of CAS wave functions, were discarded. Calculated product branching fractions are given in Table 1, together with a comparison with experiments and previous calculations. Results show that the (OH + 2H) products dominate, although the fractions for the two energy-preferred channels are moderate. Among 500 trajectories, only one case leads to the (O + H + H_2) products. Our calculations are in good agreement with experimental results,[28−31] especially the recent heavy-ion storage ring ones.[30,31] These results all show an apparent difference from the flowing afterglow measurements.[3,46] The discrepancy may be caused by the data interpretation that was employed in order to obtain the product branching ratios from two different measurements.[3,46]

The SECH MD study also outperforms the previous theoretical calculations.[21,22] Tachikawa[21] predicted 100% of H_2O + H in the DR of H_3O^+ because only the electronic ground-state of H_3O was included in his MD study and the electron excess energy was totally removed. Indeed, as shown in Figure 2, the excess energy to the ground state (that is equal to the vertical affinity potential of H_3O^+) is as large as about 5.2 eV. Such an amount of energy is able to break any O−H bond in the H_3O molecule. As expected, vertical affinity potentials become smaller when the resulting neutral molecule is in an excited state. The affinity potentials are about 1.83 and 2.45 eV for the first and second excited states, respectively. Therefore, they can play an important role in molecular dynamics simulations. The importance had been addressed by Kayanuma et al.[22] for the DR of H_3O^+. In order to consider the electron excess energy (partially in general), they started trajectories on one Rydberg state of H_3O. As a result, the product branching ratios were substantially improved as shown in Table 1. Nevertheless, the product branching fraction for OH + 2H was largely overestimated because trajectories had to roll down from the Rydberg state to valence states step-by-step in the MD simulations.[22] Such a DR mechanism may not be true for all DR trajectories of H_3O^+. Most recently, the DR of H_3O^+ has been studied by Mann et al.[24] in terms of the H_3O^+ + Cs reaction. They obtain a dominant channel of H_2O + H with a minor one of OH + H_2. These results really show an important environment effect on the product branching ratios of H_3O^+ DR as previous work.[32,47]

Since hydrogen atoms are the major species in the DR of H_3O^+, it is interesting to analyze their kinetic energy distribution that is displayed in Figure 3. It clearly shows a bimodal distribution. Actually, the bimodal profile reveals two different pathways to produce hydrogen atoms. The fast hydrogen atoms with a kinetic energy larger than 3.5 eV are directly eliminated on the electronic ground state of H_3O. In such a mechanism, the resulting H_2O molecules are vibrationally cold. On the other hand, the first eliminated hydrogen atom could be slow so that the corresponding H_2O moiety is often hot. In some circumstances, the hot H_2O moiety may have enough internal energy to dissociate into H + OH. Such a unimolecular reaction normally produces a vibrationally cold OH radical and a slow H atom. A typical trajectory is illustrated in Figure 4a. The first H escapes at about 14 fs, and the resulting H_2O is highly vibrationally excited. It has survived for 88 fs and eventually dissociates into OH and H at time t = 102 fs. Compared to the DR of H_3O^+ $(H_2O)_n$ cluster ions,[32,47] the sequential H elimination mechanism rarely happens because of the microsolvation effect.

TABLE 1: Calculated Product Branching Fractions for the Dissociative Recombination of H_3O^+ with Zero Kinetic Energy Electrons, Together with a Comparison with Experiments and Previous Theoretical Calculations

products	this work	calc[22]	calc[21]	expt[31]	expt[30]	expt[29]	expt[3,46]
H_2O + H	0.230	0.10	1.0	0.18	0.25	0.33	0.05
OH + H_2	0.108	0.015	0.0	0.11	0.14	0.18	0.36
OH + 2H	0.660	0.87	0.0	0.67	0.60	0.48	0.29
O + H + H_2	0.002	0.015	0.0	0.04	0.01	0.01	0.30

In addition, it was found that the major peak at 1.5 eV in Figure 3 results from the simultaneous eliminations of two hydrogen atoms on the first excited state of H_3O. A typical trajectory is displayed in Figure 4b. The hydrogen elimination starts at t = 11.35 fs, and the two H atoms fly away with noticeable speeds. Indeed, it is the most important mechanism for the dissociative recombination of H_3O^+. Nearly three-quarters of the hydrogen atoms are formed via this DR mechanism.

In order to clearly demonstrate the DR mechanism in Figure 4b, we have plotted the tag for the propagating state and its

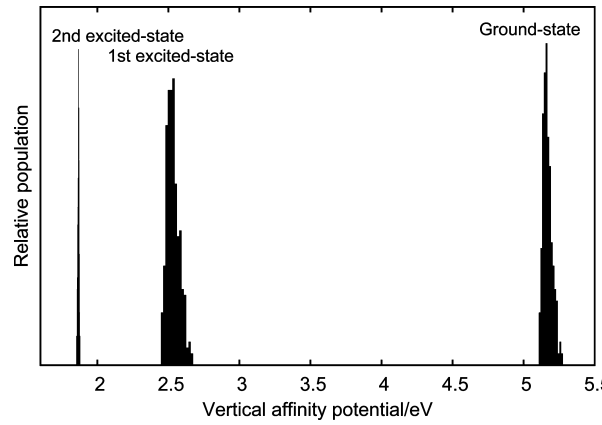

Figure 2. Vertical affinity potentials (E_{AP}^V) of the H_3O^+ ion to the ground or excited states of H_3O calculated with the 500 trajectories whose initial geometries were sampled according to the vibrational normal modes of H_3O^+ at room temperature. The third excited state of H_3O always lies above the ground state of H_3O^+ at those geometries.

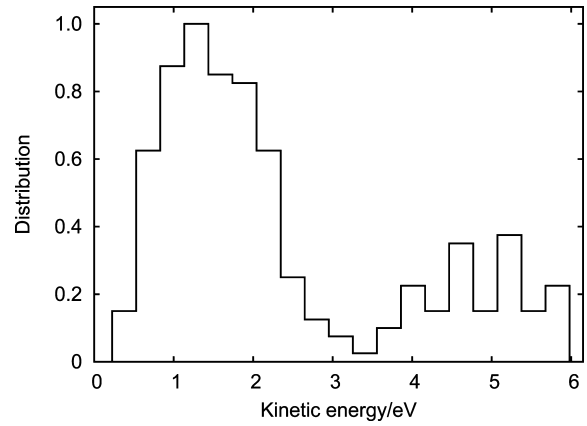

Figure 3. Distribution of kinetic energies of eliminated hydrogen atoms in DR of H_3O^+ with electrons.

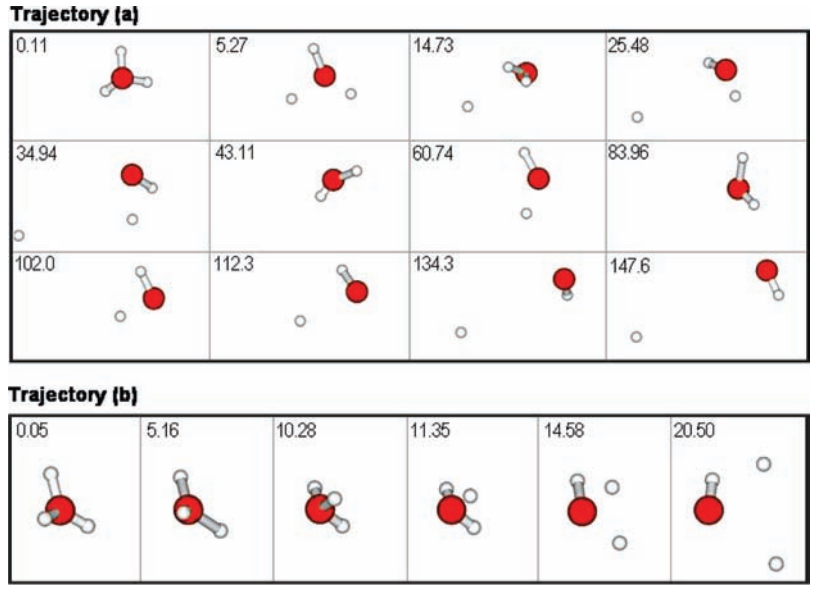

Figure 4. Two typical trajectories for the $H_3O^+ + e^- \rightarrow OH + 2H$ reaction, where the time in femtoseconds is shown in each snapshot.

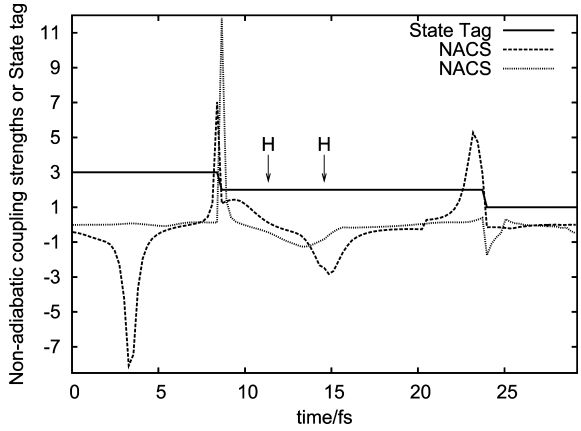

Figure 5. Tag of propagating state (solid line) and its nonadiabatic coupling strengths (dashed lines) with two adjacent states for trajectory b of Figure 4, leading to the OH + 2H products. The coupling states for NACSs will vary with the change of the propagating state as t.

nonadiabatic coupling strengths (NACS) with two adjacent states as a function of time in Figure 5. Similarly, Figure 6 shows the populations ($|c_k(t)|^2$) and the potential curves [$V_{kk}(\mathbf{R})$] of four adiabatic states. The state tag begins with the electronic ground state (i.e., state 1), then followed by the excited states in the order of energy. From Figure 5, one can see that the trajectory is initially propagated on the second excited state (i.e., state 3). At time $t = 8.4$ fs, the trajectory jumps onto the first excited state due to strong NACS. On the first excited state, two hydrogen atoms are then eliminated at nearly the same time (11.4 and 14.6 fs) indicated by the arrows. At time $t = 23.8$ fs, another surface hopping from the first excited state to the ground state occurs. However, this hopping is trivial as the system has already reached the dissociation limit of OH + H + H, which can be seen from the degenerate potential curves (labeled by the arrow at 23.8 fs) in Figure 6. The plot of potential curves also indicates that the first surface hopping happens when the second excited state has been close to the first excited state. The repulsive feature of the first excited state beginning at $t =$ 11.4 fs (just after the first trajectory surface hopping) really reveals that a large amount of energy will be released in translational energy. This feature is consistent with the kinetic energy distribution of eliminated hydrogen atoms discussed

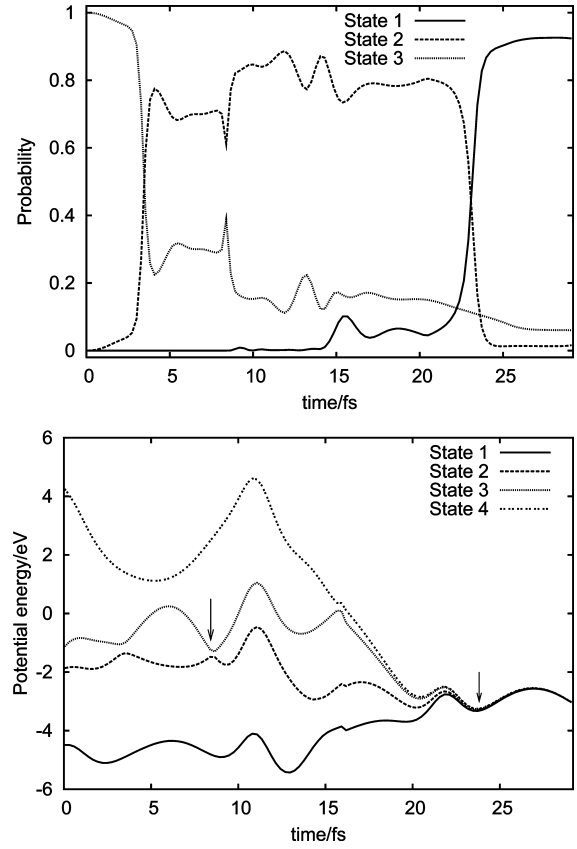

Figure 6. State populations (upper panel) and potential energies (lower panel) of four electronic states as a function of time for trajectory b of Figure 4. The two arrows denote the times when trajectory surface hopping occurs.

above. Furthermore, the trajectory surface hopping events are also demonstrated by the time evolution of state probabilities in Figure 6.

It is very interesting to study the mechanism of formation of H_2 in products since the hydrogen atoms in H_3O are covalently bound with oxygen and are well separated from each other. A typical trajectory for the $H_3O^+ + e^- \rightarrow OH + H_2$ reaction is shown in Figure 7. One can see that the H_2 molecule is formed after the two hydrogen atoms have broken their covalent bonds

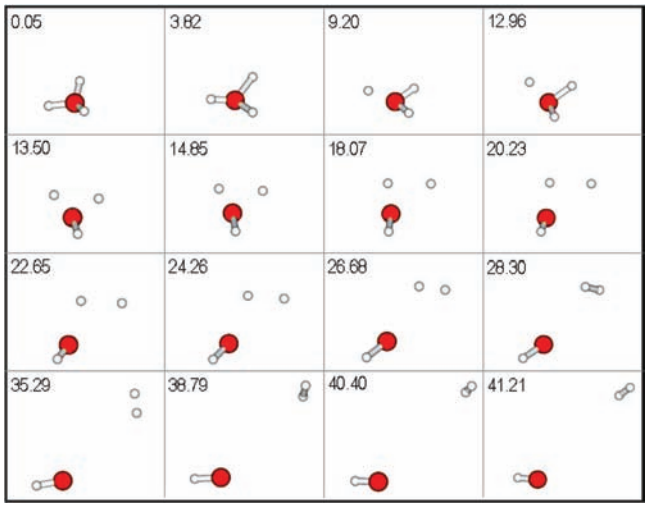

Figure 7. Typical trajectory for the $H_3O^+ + e^- \rightarrow OH + H_2$ reaction, where the time in femtoseconds is shown in each snapshot.

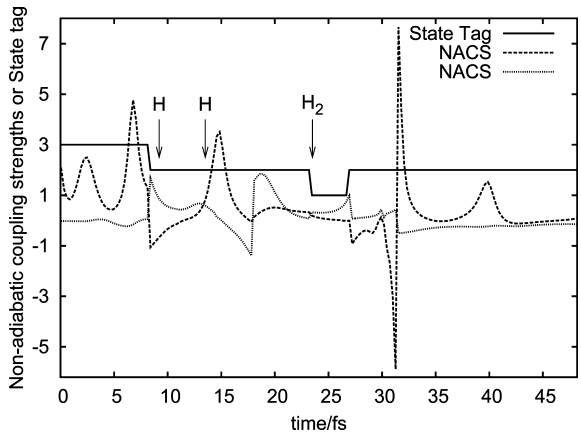

Figure 8. Tag of propagating state (solid line) and its nonadiabatic coupling strengths (dashed lines) with two adjacent states for the trajectory to the OH + H_2 products in Figure 7.

with the oxygen. In particular, these two hydrogen atoms should be eliminated on the same side and escape in the same direction with similar velocities. Under these circumstances, the nuclear distance between the two hydrogen atoms will not increase with time during the dissociation course. As a result, the two hydrogens have a chance to form a H_2 molecule by using their radical−radical attractive forces at large distances from the OH residue. Otherwise, the products would be OH + 2H instead of OH + H_2. Therefore, the formation of the H_2 product is mainly determined by the dynamics conditions. This may also imply that the product branching fraction for OH + H_2 is not large because the dynamic effects are more or less coincident.

Owing to the requirement of simultaneous elimination of two hydrogen atoms for forming H_2, the OH + H_2 products are produced only on excited states, especially on the first excited state. This has been clearly illustrated by the propagating state and the strong and complicated nonadiabatic coupling strengths versus time in Figure 8. The remarkable nonadiababatic effects are also reflected in the state populations shown in the upper panel of Figure 9. The three low-lying states are substantially mixed as a function of time. Furthermore, the potential curves in Figure 9 show that the dissociation asymptote of the OH + H_2 products is approached at time $t = 22.5$ fs. At longer times, the doubly degenerate states are due to the $X^2\Pi$ state of OH, and the severe oscillatings of potentials are created by the vibrationally hot H_2. The third state correlates to the first excited

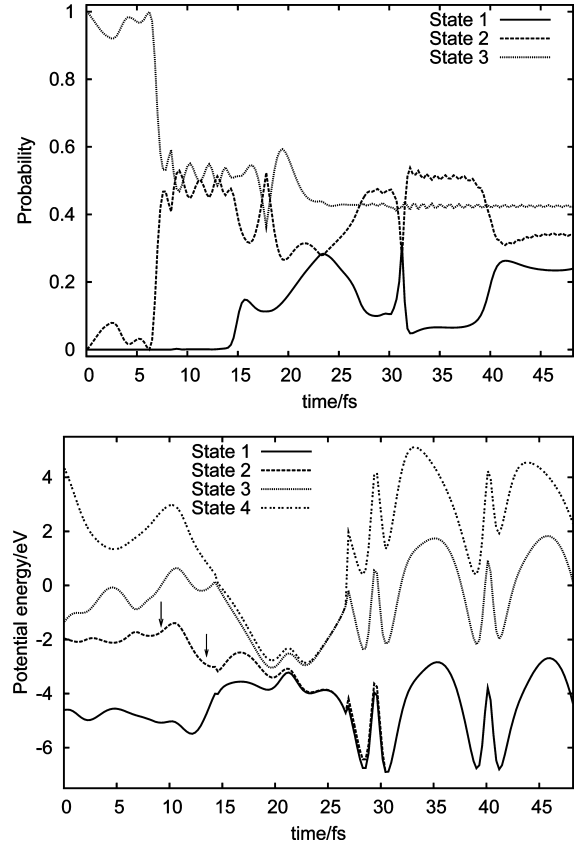

Figure 9. State populations (upper panel) and potential energies (lower panel) of four electronic states as a function of time for the trajectory in Figure 7. The two arrows refer to the times for hydrogen eliminations.

state ($A^2\Sigma$) of OH, while the highest one corresponds to the $B^1\Sigma_u^+$ state of H_2. The hot H_2 products are characteristic because they are formed at relatively large nuclear distances during the dissociation process. From the 55 trajectories forming H_2, we can estimate an average vibrational energy of 3.2 eV for H_2. But a reliable distribution of vibrational energies could not be obtained because of the small number of trajectories.

Finally, all trajectories demonstrate that DR of H_3O^+ with electrons is ultrafast and finishes within 30 fs.

4. Summary

Dissociative recombination of H_3O^+ with electrons at zero collision energy has been revisited by use of a spherical electron cloud hopping (SECH) molecular dynamics (MD) method. In the calculations, the direct ab initio MD approach was employed, where the energies, forces, and nonadiabatic coupling strengths used in trajectories were evaluated by the state-average complete active self-consistent field theory CAS(7,6) with the 6-311G(d,p) basis set. Nonadiabatic effects were treated with a surface hopping algorithm. Results show that the electron excess energy plays a crucial role in determining the product branching ratios for DR of H_3O^+. The calculated product branching ratios are in good agreement with recent experimental results. Our results also outperform previous molecular dynamics studies. The DR mechanisms have been investigated in detail for both the OH + 2H and the OH + H_2 products. It was found that the role of the first excited state of H_3O is prominent in DR of H_3O^+. In addition, the SECH MD method is applicable for studying the electron attachment of neutral molecules.[48,49]

In this work, molecular dynamics calculations were carried out by the surface hopping method. Some important quantum

effects such as quantum interference, tunneling, and leakage of zero-point energies may not be well described. To alleviate those problems, the ab initio multiple spawning trajectory method of Martinez et al.[50,51] can be used. Second, in order to study the energy dependence of DR product branching ratios, one has to know the energy-dependent electronic widths of those accessible electronic states of the neutral molecule for a DR system. The initial transition probablities could be strongly affected by the widths, especially at the resonance scattering energies. They can be calculated by a quantum dynamics method[7] for a given geometry of the cation. Such a work is in progress.

Acknowledgment. This work was performed at Brookhaven National Laboratory under Contract DE-AC02-98CH10886 with the U.S. Department of Energy and was supported by its Division of Chemical Sciences, Office of Basic Energy Sciences.

References and Notes

(1) Mitchell, J. B. A.; Rowe, C. R. *Int. Rev. Phys. Chem.* **1997**, *16*, 201.
(2) Zubarev, R. A.; Haselmann, K. F.; Budnik, B.; Kjeldsen, F.; Jensen, F. *Eur. J. Mass Spectrom.* **2002**, *8*, 337.
(3) Adams, N. G.; Poterya, V.; Babcock, L. M. *Mass Spectrom. Rev.* **2006**, *25*, 798.
(4) Florescu-Mitchell, A. I.; Mitchell, J. B. A. *Phys. Rep.* **2006**, *430*, 277.
(5) Thomas, R. D. *Mass Spectrom. Rev.* **2008**, *27*, 485.
(6) For example, see J. Phys. Conf. Ser. 4, 2005.
(7) *Mathematical and Computational Methods in R-Matrix Theory*; Plummer, M., Gorfinkiel, J. D., Tennyson, J., Eds.; CCP2: Warrington, U.K., 2007.
(8) Takagi, H. *Phys. Rev. A* **2004**, *70*, 022709.
(9) *Molecular Applications of Quantum Defect Theory*; Jungen, Ch., Ed.; Taylor & Francis Group: Oxon, U.K., 1996.
(10) Herzenberg, A. *Phys. Rev.* **1967**, *160*, 80.
(11) Birwistle, D. T.; Herzenberg, A. *J. Phys. B* **1971**, *4*, 53.
(12) Orel, A. E.; Kulander, K. C. *Phys. Rev. Lett.* **1993**, *71*, 4315.
(13) Orel, A. E. *Phys. Rev. A* **2000**, *62*, 020701.
(14) Larson, A.; Orel, A. E. *Phys. Rev. A* **2005**, *72*, 032701.
(15) Larson, A.; Orel, A. E. *Phys. Rev. A* **2001**, *64*, 062701.
(16) McCurdy, C. W.; Turner, J. L. *J. Chem. Phys.* **1983**, *78*, 6773.
(17) Greene, C. H.; Kokoouline, V. *Philos. Trans. R. Soc., Part A* **2006**, *364*, 2965.
(18) Santos, S. F. D.; Kokoouline, V.; Greene, C. H. *J. Chem. Phys.* **2007**, *127*, 124309.
(19) Hotop, H.; Ruf, M.-W.; Allan, M.; Fabrikant, I. I. *Adv. At. Mol. Opt. Phys.* **2003**, *49*, 85.
(20) Larsson, M.; McCall, B. J.; Orel, A. E. *Chem. Phys. Lett.* **2008**, *462*, 145.
(21) Tachikawa, H. *Phys. Chem. Chem. Phys.* **2000**, *2*, 4327.
(22) Kayanuma, M.; Taketsugu, T.; Ishii, K. *Chem. Phys. Lett.* **2006**, *418*, 511.
(23) Kayanuma, M.; Taketsugu, T.; Ishii, K. *Theor. Chim. Acta* **2008**, *120*, 191.
(24) Mann, J. E.; Xie, Z.; Savee, J. D.; Bowman, J. M.; Continetti, R. E. *J. Chem. Phys.* **2009**, *130*, 041102.
(25) Tachikawa, H. *Phys. Chem. Chem. Phys.* **1999**, *1*, 4925.
(26) Taketsugu, T.; Tajima, A.; Ishii, K.; Hirano, T. *Astrophys. J.* **2004**, *608*, 323.
(27) Tachikawa, H.; Orr-Ewing, A. J. *J. Phys. Chem. A* **2008**, *112*, 11575.
(28) Andersen, L. H.; Heber, O.; Kella, D.; Psdersen, H. B.; Vejby-Christensen, L.; Zajfman, D. *Phys. Rev. Lett.* **1996**, *77*, 4891.
(29) Vejby-Christensen, L.; Andersen, L. H.; Heber, O.; Kella, D.; Pedersen, H. B.; Schmidt, H. T.; Zajfman, D. *Astrophys. J.* **1997**, *483*, 531.
(30) Jensen, M. J.; Bilodeau, R. C.; Safvan, C. P.; Seiersen, K.; Andersen, L. H.; Pedersen, H. B.; Heber, O. *Astrophys. J.* **2000**, *543*, 764.
(31) Neau, A.; Al Khalili, A.; Rosen, S.; Le Padellec, A.; Derkatch, A. M.; Shi, W.; Vikor, L.; Larsson, M.; Nagard, M. B.; Andersson, K.; et al. *J. Chem. Phys.* **2000**, *113*, 1762.
(32) Yu, H.-G. *J. Chem. Phys.* **2008**, *128*, 194106.
(33) Yu, H.-G.; Muckerman, J. T. *J. Phys. Chem. A* **2004**, *108*, 8615.
(34) Yu, H.-G.; Muckerman, J. T. *J. Phys. Chem. A* **2005**, *109*, 1890.
(35) Yu, H.-G. *Chem. Phys. Lett.* **2007**, *441*, 20.
(36) Tully, J. C. *J. Chem. Phys.* **1990**, *93*, 1061.
(37) Yu, H.-G.; Muckerman, J. T. *J. Phys. Chem. A* **2004**, *108*, 10844.
(38) Werner, H.-J.; Knowles, P. J. *J. Chem. Phys.* **1985**, *82*, 5053.
(39) Krishnan, R.; Binkley, J. S.; Seeger, R.; Pople, J. A. *J. Chem. Phys.* **1980**, *72*, 650.
(40) Massey, H. S. W. *Rep. Prog. Phys.* **1949**, *12*, 248.
(41) Guberman, S. L. *Nature* **1987**, *327*, 408.
(42) Guberman, S. L. *Planet. Space Sci.* **1988**, *36*, 47.
(43) Watts, J. D.; Gauss, J.; Bartlett, R. J. *J. Chem. Phys.* **1993**, *98*, 8718.
(44) Dunning, T. H. *J. Chem. Phys.* **1989**, *90*, 1007.
(45) MOLPRO is a package of ab initio programs written by H.-J. Werner and P. J. Knowles with contributions from J. Almlof, R. D. Amos, A. Berning.
(46) Williams, T. L.; Adams, N. G. *Mon. Not. R. Astron. Soc.* **1996**, *282*, 413.
(47) Ojekull, J.; Andersson, P. U.; Nagard, M. B.; Pettersson, J. B. C.; Markovic, N.; Derkatch, A. M.; Neau, A.; Khalili, A.; et al. *J. Chem. Phys.* **2007**, *127*, 194301.
(48) Garrett, B. C.; Dixon, D. A.; et al. *Chem. Rev.* **2005**, *105*, 355.
(49) Savee, J. D.; Mozhayskiy, V. A.; Mann, J. E.; Krylov, A. I.; Continetti, R. E. *Science* **2008**, *321*, 826.
(50) Martinez, T. J. *Acc. Chem. Res.* **2006**, *39*, 119.
(51) Levine, B. G.; Coe, J. D.; Virshup, A. M.; Martinez, T. J. *Chem. Phys.* **2008**, *347*, 3.

JP902063W